Translational Oncology
www.transonc.com

Volume 9 Number 3 June 2016 pp. 228–235 228

Magnetic Resonance Imaging Identifies Differential Response to Pro-Oxidant Chemotherapy in a Xenograft Model[1]

Terry H. Landowski*, Gerald P. Guntle*, Dezheng Zhao*, Bhumasamudram Jagadish†, Eugene A. Mash†, Robert T. Dorr‡ and Natarajan Raghunand§

*University of Arizona Cancer Center, The University of Arizona, Tucson, AZ 85724, USA; †Department of Chemistry and Biochemistry, The University of Arizona, Tucson, AZ 85724, USA; ‡Department of Pharmacology, The University of Arizona, Tucson, AZ 85724, USA; §Moffitt Cancer Center, Tampa, FL 33612, USA

Abstract

Induction of oxidative stress is a key component of cancer therapy. Pro-oxidant drugs have been demonstrated to enhance the efficacy of radiotherapy and chemotherapy. An emerging concept is that therapeutic outcomes are dictated by the differential redox buffering reserve in subpopulations of malignant cells, indicating the need for noninvasive biomarkers of tumor redox that can be used for dose identification and response assessment in a longitudinal setting. Magnetic resonance imaging (MRI) enhanced with the thiol-binding contrast agent Gd-LC6-SH, and hemodynamic response imaging (HRI) in combination with hypercapnia and hyperoxia were investigated as biomarkers of the pharmacodynamics of the small molecule pro-oxidant imexon (IMX). Human multiple myeloma cell lines 8226/S and an IMX-resistant variant, 8226/IM10, were established as contralateral tumors in SCID mice. T1slope, an MRI measure of the washout rate of Gd-LC6-SH, was significantly lower post-IMX therapy in 8226/S tumors compared with vehicle controls, indicating treatment-related oxidization of the tumor microenvironment, which was confirmed by analysis of tumor tissue for thiols. T1slope and *ex vivo* assays for thiols both indicated a more reduced microenvironment in 8226/IM10 tumors following IMX therapy. HRI with hypercapnia challenge revealed IMX inhibition of vascular dilation in 8226/S tumors but not 8226/IM10 tumors, consistent with decreased immunohistochemical staining for smooth muscle actin in treated 8226/S tumors. MRI enhanced with Gd-LC6-SH, and HRI coupled with a hypercapnic challenge provide noninvasive biomarkers of tumor response to the redox modulator imexon.

Translational Oncology (2016) 9, 228–235

Introduction

Oxygen free radicals, or reactive oxygen species (ROS), are by-products of normal mitochondrial metabolism [1]. Historically, ROS, such as superoxide anion ($O_2^{\cdot -}$), hydrogen peroxide (H_2O_2), and the hydroxyl radical ($OH^{\cdot}$), have been recognized for their role in age-related damage of proteins, lipids, and DNA. More recently, studies have identified ROS as key second messengers that can activate signaling pathways to drive essential physiological functions, including cell division, migration, metabolic activity, and programmed cell death. The intracellular activity of ROS in signal transduction and the overall redox status of the cell are tightly regulated by endogenous antioxidant systems. An imbalance of the redox system in tumor cells has been identified as a potential therapeutic target for anticancer drugs [2,3].

Imexon (IMX) is an aziridine-containing iminopyrrolidone that is in phase II clinical trials for various malignancies [4–8]. Previous studies have demonstrated that IMX reacts with sulfhydryl groups

Address all correspondence to Natarajan Raghunand, Ph.D., Moffitt Cancer Center, 12902 Magnolia Drive, Tampa, FL 33612, U.S.A.
E-mail: Natarajan.Raghunand@moffitt.org

[1] This work was funded through the following grants from the National Institutes of Health: R01-CA118359, P01-CA017094, P30-CA023074 (EMSS, TACMASS, & Imaging Cores), and P30-CA076292 (IRAT & Tissue Cores).
Received 2 February 2016; Revised 16 April 2016; Accepted 23 April 2016

1936-5233/16
http://dx.doi.org/10.1016/j.tranon.2016.04.007

resulting in a decrease of intracellular thiols, an accumulation of ROS, loss of mitochondrial membrane potential, and apoptosis [9–11]. Biochemical analyses have shown that this interaction occurs via classical aziridine ring opening to bind glutathione (GSH) or via nucleophilic attack at the cyclic amidine moiety by the sulfur atom in cysteine [12].

Inactivation of common chemotherapeutic agents, such as platinum drugs, nitrogen mustards, doxorubicin, and nitrosoureas, can occur via conjugation of reduced glutathione with electrophilic centers of these molecules. Through hydrogen donation, sulfhydryl-containing species such as cysteine and GSH can also effect repair of DNA damage produced by ionizing radiation [13]. Therapeutic agents such as IMX that deplete tumor thiol reserves may therefore enhance the anticancer efficacies of both chemotherapy and radiotherapy. In a recently concluded phase 2 study, patients with relapsed/refractory B-cell non-Hodgkin lymphoma were treated with IMX as a single agent. Progression-free survival was calculated, and clinical response was correlated with a redox signature score that was generated from gene expression analyses of both pretreatment tumor biopsies and pre- and posttreatment peripheral blood mononuclear cells [4]. These laboratory correlates demonstrated that patients with higher redox scores were more likely to respond to the pro-oxidant IMX. However, no reliable method currently exists for measuring intratumoral oxidative stress directly and accurately that would allow *a priori* prediction of patient response. There is a clinical need for a noninvasive correlate of oxidative stress to inform treatment selection, monitor tumor response longitudinally, and assess spatial heterogeneity in solid tumors. The objectives of this study were therefore to develop imaging biomarkers of the pharmacodynamics of IMX and to relate our findings to differences in the responses of drug-sensitive and drug-resistant tumors to IMX.

Gd-LC6-SH is a thiol-bearing DOTA complex of gadolinium, and we have previously demonstrated that the decrease in tumor longitudinal relaxation time produced on magnetic resonance imaging (MRI) by Gd-LC6-SH at 60 minutes postinjection (= ΔT1) was correlated with tumor thiol content in Mia-PaCa-2 pancreatic and NCI-N87 gastric cancer xenografts [14]. A limitation to the interpretation of tumor ΔT1 in terms of tumor redox status is that it would also be a function of tumor perfusion that delivers the agent and its extracellular volume of distribution within the tumor. Gd-LC6-SH binds to plasma albumin at the conserved Cys^{34} site, which prolongs its retention in the tumor microenvironment. The washout rate of Gd-LC6-SH from the tumor will be a function of the local concentration of small molecule thiols that compete for binding to albumin at the same site. We hypothesize that the rate of change of tumor T1 during washout of Gd-LC6-SH (= T1slope) is a biomarker of tumor redox status that is independent of tumor perfusion and extracellular distribution volume fraction; faster washout rates will be expected in more reducing microenvironments.

In this study, we report that the T1slopes of IMX-sensitive 8226/S and IMX-resistant 8226/IM10 multiple myeloma tumor xenografts measured *in vivo* in control and IMX-treated mice correlate with tumor thiol content measured *ex vivo* using histologic and enzymatic assays. Treatment of 8226/IM10 tumors with the pro-oxidant IMX produced a trend toward a more reduced tumor microenvironment, suggesting a compensatory response in these IMX-resistant tumors. We also report that hemodynamic response imaging (HRI) by MRI in combination with hypercapnia provides a noninvasive biomarker for the effect of IMX on tumor vascular maturation. We discuss the potential for Gd-LC6-SH MRI and HRI in pretherapy prognostication and posttherapy response assessment.

Materials and Methods

Mice, Tumors, and Drug

All animal experiments were conducted in accordance with the guidelines of the Institutional Animal Care and Use Committee at the University of Arizona. The 8226/S human myeloma cells were originally obtained from ATCC, and the IMX-resistant 8226/IM10 cell line was created by continuous exposure to IMX as previously described [15,16]. Dual xenografts on contralateral flanks of 6-week-old female SCID mice were established by subcutaneous injection of 10×10^6 cells. Animals were monitored every 3 days for general health, body weight, and tumor volume by caliper measure. Mean tumor volume was used to stratify animals into equal treatment groups when the tumors were approximately 100 to 250 mm^3. IMX was generously provided by AmpliMed Corp, Tucson, AZ, and was prepared as a 15-mg/ml solution in 0.9% NaCl. Animals were administered either IMX (150 mg/kg, intraperitoneally [i.p.]) or saline (0.25 ml per 25 g, i.p.) on a day 1-5-9 schedule. MRI was done on day 0 (pretreatment) and 2 hours post drug administration on day 9.

Hemodynamic Response Imaging

All MRI measurements were made on a Bruker Biospec MR imager with a 7-T horizontal bore magnet equipped with 600-mT/m self-shielded gradients (Bruker Biospin, Billerica, MA). Mice were anesthetized using isoflurane (1-2%, rest air) and cannulated at the tail vein for injections. T2*-weighted gradient echo (GRE) images were collected using the following parameters: repetition time (TR) = 200 milliseconds, echo time (TE) = 15 milliseconds, flip angle (FA) = 45°, matrix = 128 × 128, number of averages (NA) = 8. Six consecutive images were acquired with the mouse breathing air followed by 7 consecutive images after the breathing gas was changed to air-CO_2 (95% air, 5% CO_2) and a final 7 consecutive images acquired as the animal breathed carbogen (95% O_2, 5% CO_2). The first image acquired following each change in breathing mix was left out during data analysis to account for gas exchange and physiological equilibration. Indices of vasodilation (VD) and vascular function (VF) were calculated by the method of Abramovitch and colleagues [17,18], as follows:

$$\mathrm{VF} = \ln\left(\frac{I_{\mathrm{O2\text{-}CO2}}}{I_{\mathrm{air\text{-}CO2}}}\right)/(\mathrm{TE}\bullet C_{\mathrm{MRI}}) \quad (1)$$

$$\mathrm{VD} = \ln\left(\frac{I_{\mathrm{air\text{-}CO2}}}{I_{\mathrm{air}}}\right)/(\mathrm{TE}\bullet C_{\mathrm{MRI}}) \quad (2)$$

Here I_{air}, $I_{\mathrm{air\text{-}CO2}}$, and $I_{\mathrm{O2\text{-}CO2}}$ are the T2*-weighted MRI signal intensities with the mouse breathing the respective gas mixes. The constant C_{MRI} incorporates the effects of the magnetic field strength and the susceptibility of deoxyhemoglobin and was scaled linearly from the value calculated by Ogawa and colleagues [19] to 892 s^{-1} at 7 T.

Gd-LC6-SH MRI

{1,4,7-Tris(carboxymethyl)-10-[N-(6-mercaptohexyl)carbamoyl]-1,4,7,10-tetraazacyclododecanato}gadolinium (Gd-LC6-SH)

was synthesized as described previously [20]. Gd-LC6-SH was prepared as a 25-mM solution in injectable saline at pH 7.4 for intravenous (i.v.) administration. After acquisition of scout MR images, a precontrast T1 map and proton-density map were acquired. This was followed by a co-registered dynamic GRE series (TR = 78 milliseconds, TE = 3.5 milliseconds, FA = 75°, NA = 1, number of repetitions = 60, scan time = 20 minutes) during which the contrast medium was administered. After the start of the dynamic series, Gd-LC6-SH (0.05 mmol/kg) was administered via the tail vein cannula over 1 minute and chased with 0.15 ml of saline injected over 1 minute. After the dynamic series, 10 co-registered GRE images (TR = 78 milliseconds, TE = 3.5 milliseconds, FA = 75°, NA = 12) were acquired at regular intervals to 60 minutes after injection of Gd-LC6-SH. Together with the precontrast proton density map, these 10 postcontrast T1-weighted images were used to compute 10 postcontrast T1 maps. In oxidizing microenvironments, Gd-LC6-SH would remain bound to albumin and only be cleared slowly because of the "enhanced permeability and retention" effect. In reducing microenvironments, competitive binding by other small molecule thiols would release the Gd-LC6-SH from the albumin and accelerate its washout. The parameter ΔT1 was calculated as the difference in tumor T1 precontrast versus 60 minutes postinjection of Gd-LC6-SH (Figure 1). A larger ΔT1 would be expected in oxidizing tumor microenvironments than in reducing microenvironments. This effect on tumor ΔT1 is enhanced by the 47% higher longitudinal relaxivity (r_1) of Gd-LC6-SH when it is bound to albumin compared with the r_1 of the unbound molecule [21,22]. In addition to interstitial albumin, exofacial protein thiols could constitute another static pool of thiol-binding sites in the tumor [23,24]. The dimensionless parameter T1slope was calculated as the rate of change of tumor T1 between ~20 and 60 minutes postinjection of Gd-LC6-SH from tumor pixels that exhibited a minimum of 20% peak signal enhancement postinjection of Gd-LC6-SH (Figure 1). A larger T1slope would be expected in reducing tumor microenvironments than in oxidizing microenvironments.

Tissue Assay for Thiols

Tumors from mice in the Gd-LC6-SH MRI experiment were rapidly harvested following sacrifice by cervical dislocation under anesthesia (4% isoflurane in O_2). This was done the day after imaging to allow for complete clearance of Gd-LC6-SH from the animals. Mice were administered a fourth dose of IMX (150 mg/kg, i.p.) or saline (0.25 ml per 25 g, i.p.) 2 hours before sacrifice. Excised tumors were immediately placed into cryovials and frozen. Frozen tumor sections were stained with mercury orange and analyzed as described previously [14]. Thiol content in tumor tissue extracts was assayed using the Fluoro Thiol kit (Cell Technology Inc., Mountain View, CA). Briefly, 18 to 40 mg of tumor tissue was homogenized on ice in the supplied lysis buffer. Tumor lysates were centrifuged, and the clarified supernatant was immediately analyzed on a fluorescence plate reader with excitation at 485 nm and emission at 595 nm. Fluorescence readings were calibrated against the supplied GSH standard and normalized to sample protein content. Protein concentration in the tumor lysates was determined separately by following the standard protocol for the Pierce BCA Protein Assay Kit (Thermo Scientific, Rockford, lL).

Immunohistochemistry (IHC)

After completion of imaging on day 9, mice in the HRI experiment were kept anesthetized with isoflurane while the breathing gas was switched to air. Mice were then administered 2-nitroimidazole (pimonidazole, 60 mg/kg) via the tail vein line. After 30 minutes, the animals were sacrificed, and the tumors were harvested, fixed in formalin, and embedded in paraffin for further processing. Tissue sections were stained with hematoxylin and eosin, or assayed by IHC for detection of pimonidazole adducts (Hypoxyprobe EF5 antibody), or CD31 (Abcam ab28364), or smooth muscle actin (SMA, Abcam ab32575). Pimonidazole analysis was done by collecting color-balanced images of five independent fields (20× magnification) of each tumor. A representative cell demonstrating "minimal positive intensity" was selected, and the images were converted to gray scale using ImageJ (National Institutes of Health). Gray-scale histograms were used to determine the total pixel count over threshold in each image, and the mean positive area was calculated on each tumor. CD31- and SMA-stained slides were scanned with the Aperio ScanScope XT (Vista, CA), and positive pixel analysis was performed using Aperio Genie v1 software. Briefly, the algorithm measured staining intensity across the entire area of the tumor and classified the number of pixels containing stained tissue. The results are presented as percent positivity, which was calculated as the number of positive pixels divided by the total number of pixels multiplied by 100.

Results

Gd-LC6-SH MRI in Pro-Oxidant Chemotherapy

Tumor ΔT1 was measured before the start of treatment (day 0) and again 2 hours following a third dose of saline or IMX (day 9). In the

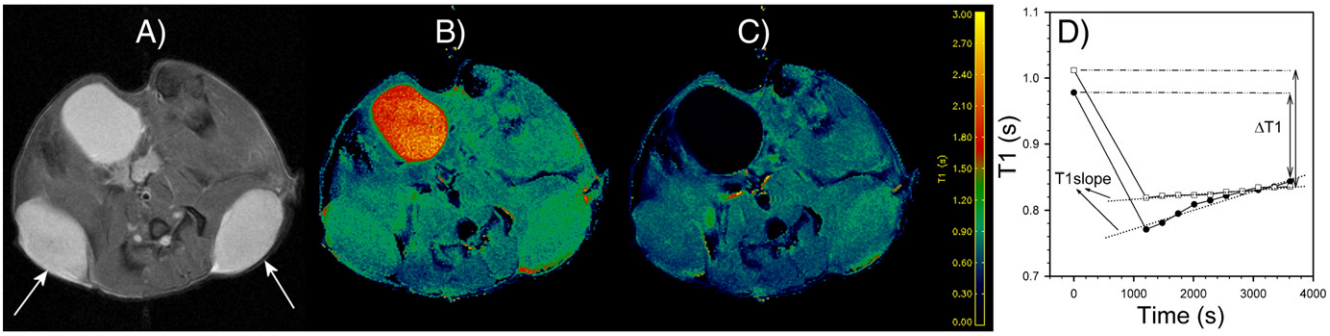

Figure 1. Example of (A) transaxial T2-weighted MR image of a mouse with arrows pointing to the dual tumors, and the corresponding (B) precontrast T1 map and (C) post-GdLC6SH T1 map. Also prominently visible is the bladder. (D) The calculation of the parameters T1 and T1slope from the temporal variation of tumor T1 following i.v. injection of Gd-LC6-SH at time zero.

8226/S tumors, ΔT1 was lower at the end of the day 1-5-9 saline treatment schedule relative to pretreatment ΔT1, although this decrease did not achieve statistical significance (Figure 2A, $P = .062$). Treatment of 8226/S tumors with IMX resulted in a significant increase in ΔT1 at the end of the day 1-5-9 treatment schedule relative to saline treatment (Figure 2*A*, $P = .007$) and a nonsignificant increase relative to pretreatment ΔT1 (Figure 2*A*, $P = .096$). 8226/IM10 tumors did not show an appreciable change in ΔT1 over the 9-day saline treatment schedule but exhibited a nonsignificant decrease in ΔT1 at the end of the IMX treatment schedule relative to saline treatment (Figure 2*A*, $P = .453$). Posttreatment versus pretreatment changes in tumor ΔT1, calculated for each animal, are summarized in Figure 2*B*.

We have also examined the parameter T1slope, which is a dimensionless measure of the washout rate of Gd-LC6-SH. T1slope did not change appreciably in either tumor type following treatment with saline. T1slope was significantly decreased in 8226/S tumors following treatment with IMX, relative to saline controls, indicating a shift toward a more oxidizing tumor microenvironment (Figure 3*A*). Consistent with this MRI finding, the thiol content of 8226/S tumors was observed to be significantly decreased by IMX treatment relative to saline controls, as measured by mercury orange staining (Figure 3*B*) and the Fluoro Thiol assay (Figure 3*C*). The T1slope of 8226/IM10 tumors was higher following treatment with IMX relative to saline controls, indicating a movement of tumor redox in the reducing direction (Figure 3*A*). Mercury orange staining and the Fluoro Thiol assay confirmed that treatment with IMX paradoxically increased thiol content in 8226/IM10 tumors (Figure 3, *B* and *C*). Although the difference in the response of 8226/IM10 tumors to saline versus IMX did not achieve statistical significance, these slight increases were consistent across all three measures: T1slope, mercury orange, and Fluoro Thiol. By all three measures, the difference in the response of the two tumor types to IMX was statistically significant (Figure 3, *A*–*C*).

Hemodynamic Response Imaging

We have computed a tumor VD from the change in T2*-weighted MRI signal intensity produced upon switching the inhaled gas from air to air-CO_2. We have also calculated the change in T2*-weighted MRI signal intensity produced by a further switch of the inhaled gas from air-CO_2 to oxygen-CO_2 and used it to compute an index of VF. An increase in VD was calculated in 8226/S tumors over the day 1-5-9 treatment with saline, indicating progressive vascular maturation during tumor growth in this period (Figure 4*A*). Treatment of 8226/S tumors with IMX produced a significant decrease in VD relative to the saline controls over this same period (Figure 4*A*, $P = .030$), indicating that IMX interferes with vascular maturation in these tumors. Tumor VD was observed to decrease in 8226/IM10 tumors over 9 days of treatment with both saline and IMX, with no significant difference between the two treatment groups in these IMX-resistant tumors (Figure 4*B*). No significant differences were found in VF between saline and IMX treatment in either 8226/S or 8226/IM10 tumors (Figure 4).

Immunohistochemistry

Mice in the HRI experiment were infused with the 2-nitroimidazole compound pimonidazole. In a complex series of bioreductive reactions catalyzed by cellular nitroreductase enzymes under conditions of hypoxia, pimonidazole forms adducts with thiol-rich macromolecules [25]. We have detected the pimonidazole-protein conjugate in formalin-fixed paraffin-embedded (FFPE) tissue sections by IHC. Mean pimonidazole staining in 8226/S and 8226/IM10 xenograft tumors from individual SCID mice treated with IMX or vehicle control is shown in Figure 5*A*, and a representative image demonstrating the pixel density defined as "positive" is shown in Figure 5*B*. IMX treatment increases pimonidazole staining in IMX-sensitive (8226/S) tumors by 2.6-fold and in IMX-resistant (8226/IM10) xenografts by 9.1-fold. We assessed the tumor microvessel density with the panendothelial marker CD31 and relative pericyte coverage by the SMA/CD31 ratio in FFPE sections from the xenograft tumors. The SMA/CD31 ratio indicated that a significantly greater proportion of the vasculature in the IMX-treated 8226/IM10 tumors is associated with pericytes, indicative of vascular maturity or normalization, relative to saline-treated control 8226/IM10 tumors (Figure 6*A*). Figure 6*B* demonstrates CD31 and SMA staining in serial sections from a representative 8226/S xenograft tumor.

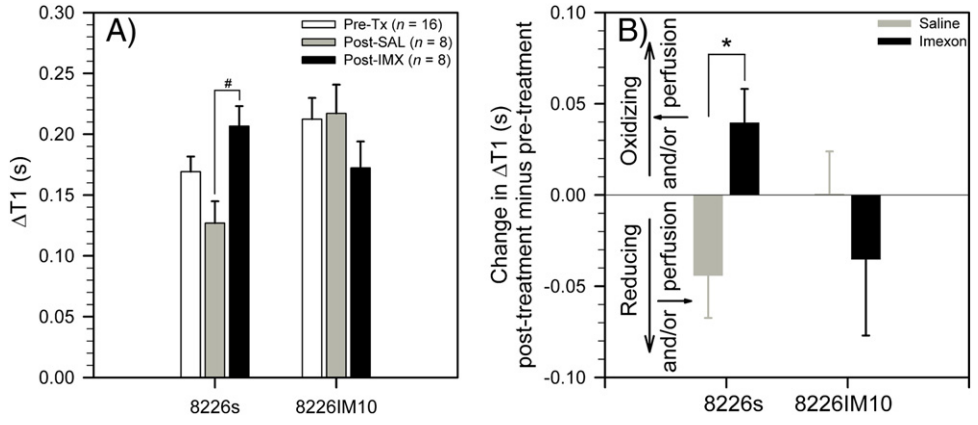

Figure 2. (A) T1 following administration of Gd-LC6-SH, measured pretherapy, postsaline, and post-IMX, in 8226/S and 8226/IM10 tumors (mean ± SEM, $^{\#}P = .007$). (B) Posttherapy versus pretherapy change of T1 following administration of Gd-LC6-SH in individual 8226/S and 8226/IM10 tumors (mean ± SEM, $n = 8$, $^{*}P = .016$).

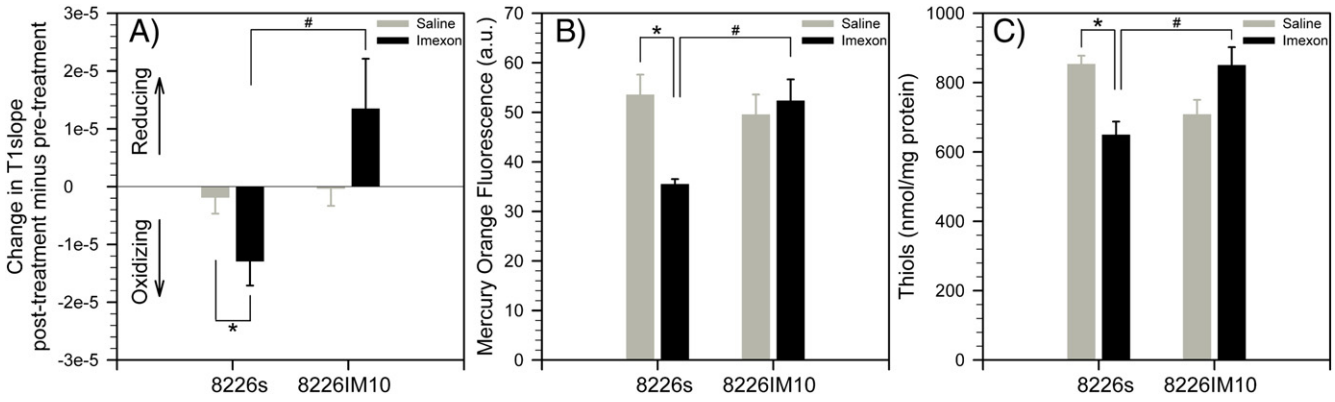

Figure 3. (A) Posttherapy versus pretherapy change of T1slope in individual 8226/S and 8226/IM10 tumors (mean ± SEM, $n = 8$, $^{*}P = .044$, $^{\#}P = .018$). (B) Mercury Orange staining for thiols in frozen sections of 8226/S and 8226/IM10 tumors following saline or IMX treatment (mean ± SEM, $n = 5$, $^{*}P = .003$, $^{\#}P = .004$). (C) Fluoro Thiol assay for thiols, normalized to protein content, in extracts of 8226/S and 8226/IM10 tumors from mice treated with saline or IMX (mean ± SEM, $n = 3$, $^{*}P = .026$, $^{\#}P = .036$).

Discussion and Conclusions

Gd-LC6-SH is an MRI contrast agent that spontaneously binds to the conserved Cys^{34} residue in plasma albumin following i.v. administration. Once bound to protein, Gd-LC6-SH will be subject to the "enhanced permeability and retention" effect in tumors, whereas the unbound small molecule will be cleared relatively rapidly. The rate of washout of gadolinium from tumor will be a function of the local concentration of competing thiols that can dislodge Gd-LC6-SH from macromolecular binding sites. We have developed T1slope, the rate of change of tumor T1 during washout of Gd-LC6-SH, as a biomarker of local extracellular tissue redox status that is independent of tumor perfusion and contrast agent volume of distribution in the tumors. For example, in IMX-sensitive 8226/S tumors, the ΔT1 was measured to decrease over the 9-day treatment with saline (Figure 2*B*), whereas T1slope remained essentially unchanged over the same period (Figure 3*A*). This difference is consistent with a decrease in perfusion delivery and/or extracellular volume of distribution of Gd-LC6-SH in 8226/S tumors due to growth rather than any change in tumor extracellular redox arising from saline "treatment." The decrease in 8226/S tumor T1slope over the 9-day treatment with IMX (Figure 3*A*) points to a more oxidizing tumor microenvironment following treatment, consistent with the known pro-oxidant and thiol-reactive chemical properties of IMX. This was corroborated by *ex vivo* assays of 8226/S tumor thiol content (Figure 3, *B* and *C*). The posttherapy T1slope of IMX-resistant 8226/IM10 tumors was higher following the 9-day IMX treatment period but unchanged over the 9-day saline control regimen, although this difference was not statistically significant (Figure 3*A*). This trend indicates a more reducing microenvironment in 8226/IM10 tumors in response to IMX treatment and was mirrored in *ex vivo* assays of 8226/IM10 tumor thiol content (Figure 3, *B* and *C*). IHC of pimonidazole staining, an indirect indicator of the availability of intracellular macromolecular and nonprotein thiols, was significantly higher in FFPE sections of IMX-treated 8226/IM10 tumors than in saline-treated controls (Figure 5). These observations correlate well with our previous work demonstrating that the IMX-resistant 8226/IM10 cells have higher basal expression of antioxidant systems [15], higher levels of the intracellular antioxidant glutathione, and increased expression of glutathione peroxidase [16] relative to the parent 8226/S cell line.

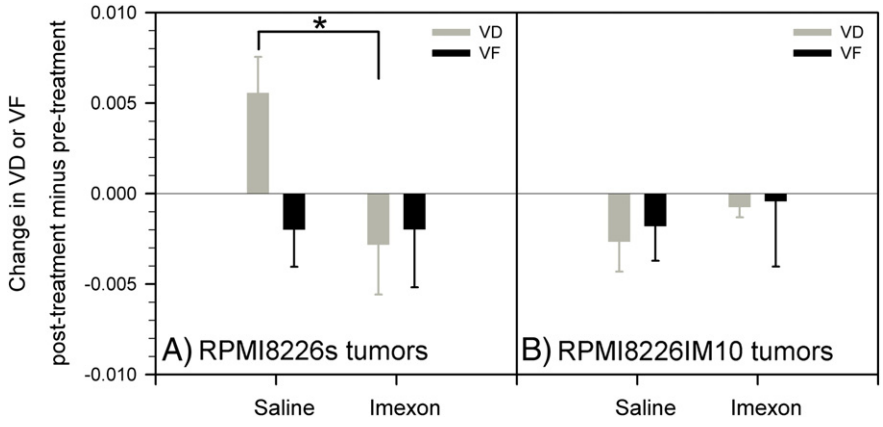

Figure 4. HRI evaluation of VD (using hypercapnia, dimensionless) and VF (using hyperoxia, dimensionless) in IMX-sensitive 8226/S and IMX-resistant 8226/IM10 tumors grown as contralateral xenografts in SCID mice treated with either saline or IMX (mean ± SEM, $n = 5$). A significant decrease in VD was observed following IMX treatment relative to saline controls in only the 8226/S tumors ($^{*}P = .030$).

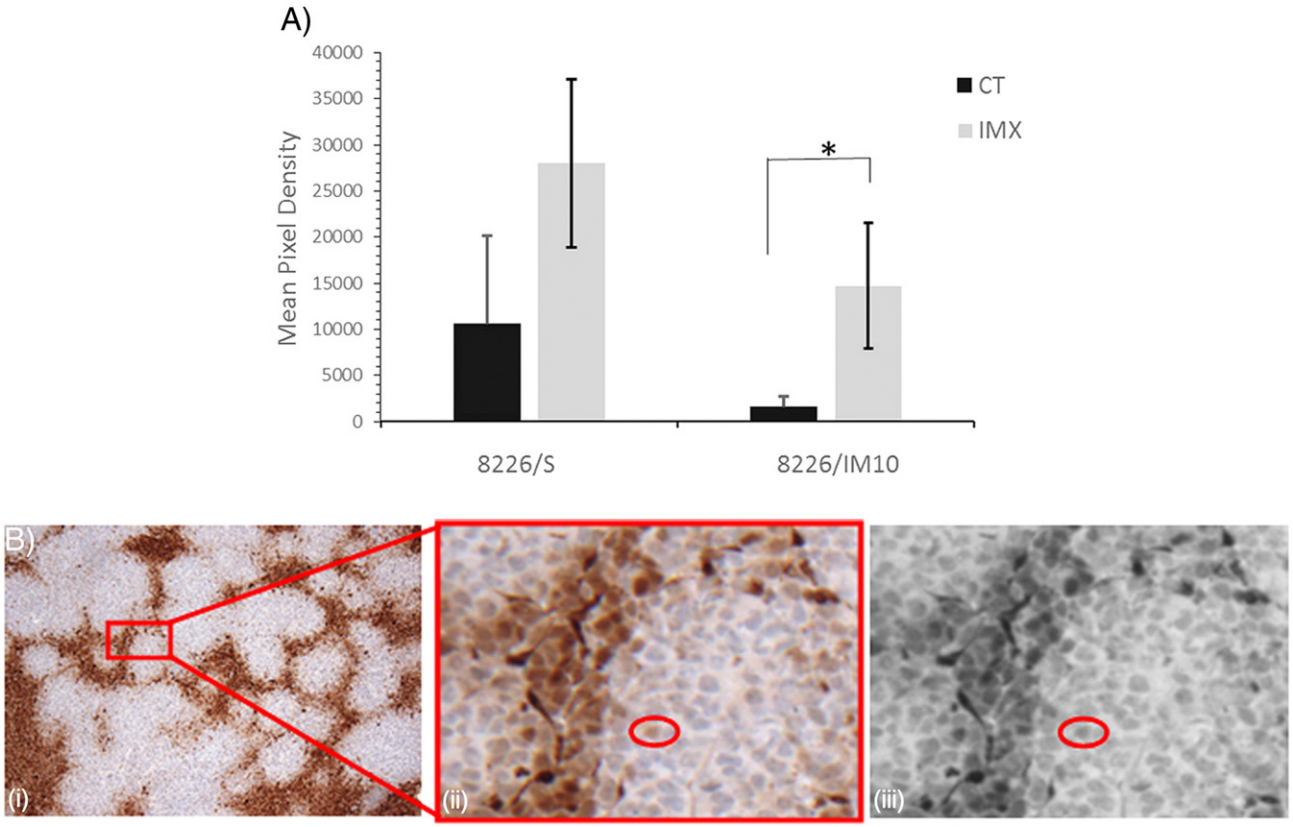

Figure 5. Immunohistochemistry of pimonidazole staining in IMX-sensitive 8226/S and IMX-resistant 8226/IM10 tumors grown in SCID mice treated with either saline (CT, control) or IMX. (A) Mean pixel density above threshold of pimonidazole staining in FFPE tissue ($n = 5$ images per slide). (B) Representative image of 8226/S tumor following EF5 staining. (i) 10× image. (ii) Inset demonstrating "minimum positive cell" used to determine threshold for quantitative analysis. (iii) Gray-scale conversion of (ii).

This may lead to a "priming" effect that allows a greater compensatory response in resistant cells that is triggered by IMX challenge. An imaging method to monitor the degree and spatial extent of such a compensatory response within a tumor subpopulation will enable the oncologist to adapt therapy and circumvent the onset of resistance.

The plasma half-life of IMX in mice is 12 to 15 minutes after intraperitoneal injection [26], and in these experiments, we injected Gd-LC6-SH into the mice 2 hours after the IMX to minimize direct reaction between the two species. Another concern is whether IMX treatment decreases the availability of albumin-Cys^{34} and what effect this might have on the utility of tumor ΔT1 and T1slope as measures of tumor redox. Albumin-Cys^{34} exists in two major forms in plasma, as the thiolate anion albumin-Cys^{34}-S$^-$ and as a mixed disulfide albumin-Cys^{34}-S-S-X where X might be a small molecule thiol such as cysteine or homocysteine. The careful work of Jacobsen and colleagues on the binding of homocysteine to albumin [27] suggests that Gd-LC6-SH would react primarily with albumin-Cys^{34}-S-S-X in a redox-neutral exchange rather than participate in oxidative disulfide bond formation with albumin-Cys^{34}-S$^-$ that is likely to be slow relative to the *in vivo* clearance times of unbound Gd-LC6-SH. Although IMX may be expected to have some reactivity toward albumin-Cys^{34}-S$^-$, it does not react readily with disulfides [12] and would therefore not be expected to decrease availability of albumin-Cys^{34}-S-S-X as a target for binding of Gd-LC6-SH. A practical concern when measuring T1slope is the need to image for a long period (60 minutes) following injection of the contrast agent; this is necessitated by the time required for a significant change in tumor T1 to manifest following gadolinium washout. For a given change in tumor gadolinium concentration, a proportional change in tumor relaxation rate (R1 = 1/T1) is produced, with the proportionality constant being the r_1 relaxivity of the gadolinium. Our ongoing work is focused on developing variants of Gd-LC6-SH with higher r_1 relaxivities when bound to albumin, which will result in larger T1slope values for a given washout rate of tissue gadolinium, thereby decreasing the imaging time required.

Abramovitch and coworkers developed HRI driven by hypercapnia (elevated CO_2) and hyperoxia (elevated O_2) for *in vivo* assessment of vascular maturation and vascular function, respectively, in tumors and normal parenchyma [17,18]. They have argued that the change in MRI signal intensity due to hypercapnia (captured in VD) arises from a change in the apparent longitudinal relaxation time T1 due to local blood flow changes stemming from vasodilation. In contrast to mature capillaries, immature blood vessels lacking pericytes and smooth muscle cells do not dilate in response to hypercapnia, and VD has the potential to be a noninvasive reporter of vascular maturation. They have also argued that a change in MRI signal intensity due to hyperoxia (captured in VF) would stem from a change in T2* produced by changes in local deoxyhemoglobin concentration. Subject to the caveat that oxygen saturation of hemoglobin at the lungs may already be near maximal under air breathing, VF may noninvasively report on vascular function. HRI revealed that 8226/S tumors in IMX-treated mice exhibit significantly lower vasodilation

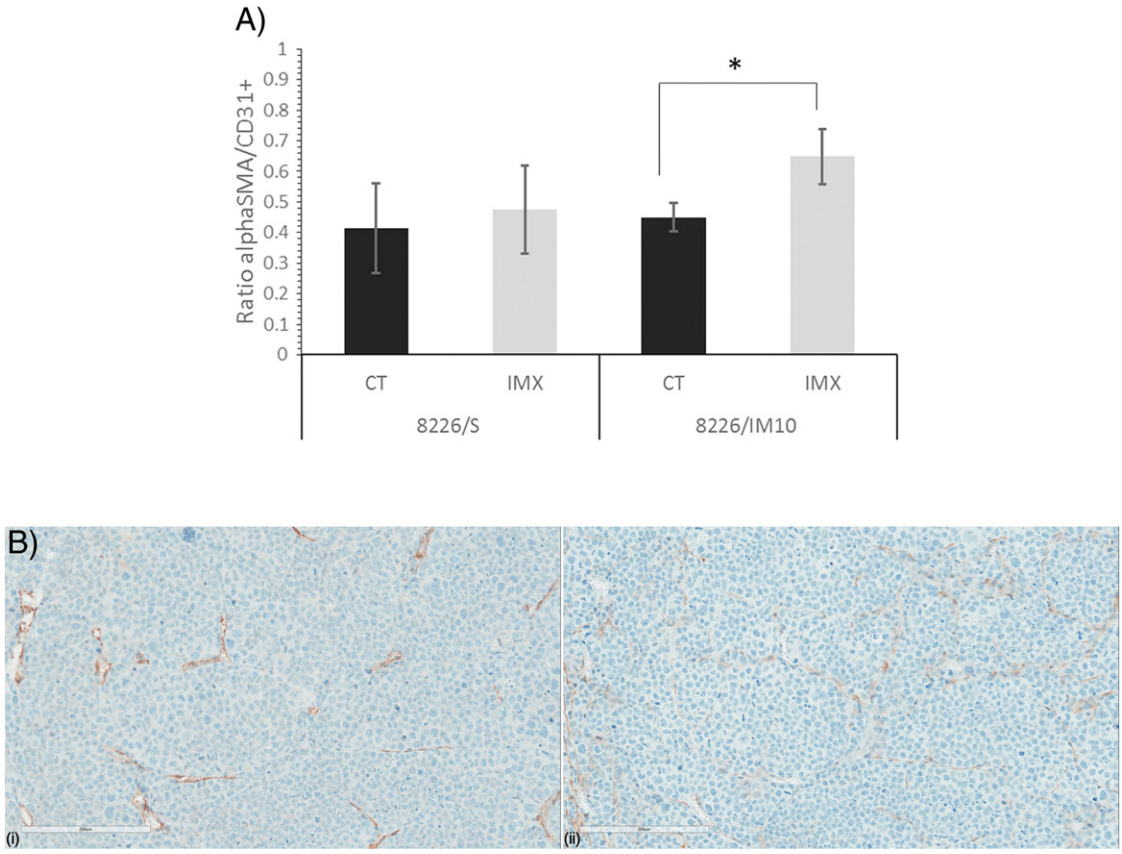

Figure 6. Immunohistochemistry of SMA and CD31 staining in IMX-sensitive 8226/S and IMX-resistant 8226/IM10 tumors grown in SCID mice treated with either saline (CT, control) or IMX. (A) Positive pixel analysis was used to determine the percent positivity across the whole area of each xenograft tumor. Data are presented as the ratio of the mean percent positivity of SMA to the mean percent positivity of CD31, ± SEM. *$P < .05$. (B). Representative serial sections from an 8226/S xenograft tumor stained for (i) CD31 and (ii) SMA.

in response to hypercapnia than in control animals. No significant differences were observed on HRI in the IMX-resistant 8226/IM10 tumors, although the ratio of SMA to CD31 staining was significantly higher in IMX-treated tumors than in saline-treated controls. This finding once again supports the contention that IMX-resistant tumors with enhanced antioxidation response system may undergo a "rebound" effect following challenge with redox-active agents. We propose that HRI perturbed with hypercapnia (air versus air-CO_2) is a clinically translatable and noninvasive marker for assessment of tumor sensitivity to IMX.

Therapies that deplete the tumor antioxidant pool can enhance chemosensitivity and radiation response. Resistance to co-therapy with redox modulators can arise from a compensatory antioxidant response by a subpopulation of tumor cells. Rational identification of the proper dose and dosing schedule for a redox modulator will require the ability to longitudinally monitor tumor redox status as well as its heterogeneity within solid tumors. In this study, we have used *in vivo* MRI to measure T1slope, the rate of change of tumor T1 during washout of Gd-LC6-SH. The T1slope of IMX-sensitive 8226/S and IMX-resistant 8226/IM10 multiple myeloma tumor xenografts in control and IMX-treated mice is predictive of tumor thiol content change with therapy, confirmed by *ex vivo* histologic and enzymatic assays for thiols. We envision clinical application for pretreatment identification of patients who are more likely to respond to redox modulators such as IMX, as well as for longitudinal assessment to enable adaptive, personalized, treatment with redox-sensitive chemotherapies and radiation with or without co-treatment with a redox modulator. In the near term, HRI in conjunction with hypercapnia provides a readily translatable and noninvasive biomarker for the longitudinal monitoring of tumor response to IMX in clinical studies. Our continuing efforts are directed at combining imaging biomarkers with pretreatment biomarkers such as the redox signature score [4] to increase the overall predictive power and guide clinical therapy.

Acknowledgements

This work was funded through the following grants from the National Institutes of Health: R01-CA118359, P01-CA017094, P30-CA023074 (EMSS, TACMASS, & Imaging Cores), and P30-CA076292 (IRAT & Tissue Cores).

Conflicts of interest: none.

References

[1] Chandel NS, McClintock DS, Feliciano CE, Wood TM, Melendez JA, Rodriguez AM, and Schumacker PT (2000). Reactive oxygen species generated at mitochondrial complex III stabilize hypoxia-inducible factor-1alpha during hypoxia: a mechanism of O2 sensing. *J Biol Chem* **275**, 25130–25138.

[2] Laurent A, Nicco C, Chereau C, Goulvestre C, Alexandre J, Alves A, Levy E, Goldwasser F, Panis Y, and Soubrane O, et al (2005). Controlling tumor growth

by modulating endogenous production of reactive oxygen species. *Cancer Res* **65**, 948–956.

[3] Wondrak GT (2009). Redox-directed cancer therapeutics: molecular mechanisms and opportunities. *Antioxid Redox Signal* **11**, 3013–3069.

[4] Barr PM, Miller TP, Friedberg JW, Peterson DR, Baran AM, Herr M, Spier CM, Cui H, Roe DJ, and Persky DO, et al (2014). Phase 2 study of imexon, a prooxidant molecule, in relapsed and refractory B-cell non-Hodgkin lymphoma. *Blood* **124**, 1259–1265.

[5] Cohen SJ, Zalupski MM, Modiano MR, Conkling P, Patt YZ, Davis P, Dorr RT, Boytim ML, and Hersh EM (2010). A phase I study of imexon plus gemcitabine as first-line therapy for advanced pancreatic cancer. *Cancer Chemother Pharmacol* **66**, 287–294.

[6] Dragovich T, Gordon M, Mendelson D, Wong L, Modiano M, Chow HH, Samulitis B, O'Day S, Grenier K, and Hersh E, et al (2007). Phase I trial of imexon in patients with advanced malignancy. *J Clin Oncol* **25**, 1779–1784.

[7] Moulder S, Dhillon N, Ng C, Hong D, Wheler J, Naing A, Tse S, La PA, Dorr R, and Hersh E, et al (2010). A phase I trial of imexon, a pro-oxidant, in combination with docetaxel for the treatment of patients with advanced breast, non–small cell lung and prostate cancer. *Invest New Drugs* **28**, 634–640.

[8] Weber JS, Samlowski WE, Gonzalez R, Ribas A, Stephenson J, O'Day S, Sato T, Dorr R, Grenier K, and Hersh E (2010). A phase 1-2 study of imexon plus dacarbazine in patients with unresectable metastatic melanoma. *Cancer* **116**, 3683–3691.

[9] Dvorakova K, Payne CM, Landowski TH, Tome ME, Halperin DS, and Dorr RT (2002). Imexon activates an intrinsic apoptosis pathway in RPMI8226 myeloma cells. *Anticancer Drugs* **13**, 1031–1042.

[10] Dvorakova K, Payne CM, Tome ME, Briehl MM, McClure T, and Dorr RT (2000). Induction of oxidative stress and apoptosis in myeloma cells by the aziridine-containing agent imexon. *Biochem Pharmacol* **60**, 749–758.

[11] Dvorakova K, Waltmire CN, Payne CM, Tome ME, Briehl MM, and Dorr RT (2001). Induction of mitochondrial changes in myeloma cells by imexon. *Blood* **97**, 3544–3551.

[12] Iyengar BS, Dorr RT, and Remers WA (2004). Chemical basis for the biological activity of imexon and related cyanoaziridines. *J Med Chem* **47**, 218–223.

[13] Bailey HH (1998). L-S, R-buthionine sulfoximine: historical development and clinical issues. *Chem Biol Interact* **111–112**, 239–254.

[14] Guntle GP, Jagadish B, Mash EA, Powis G, Dorr RT, and Raghunand N (2012). Tumor xenograft response to redox-active therapies assessed by magnetic resonance imaging using a thiol-bearing DOTA complex of gadolinium. *Transl Oncol* **5**, 190–199.

[15] Samulitis BK, Landowski TH, and Dorr RT (2006). Correlates of imexon sensitivity in human multiple myeloma cell lines. *Leuk Lymphoma* **47**, 97–109.

[16] Dvorakova K, Payne CM, Tome ME, Briehl MM, Vasquez MA, Waltmire CN, Coon A, and Dorr RT (2002). Molecular and cellular characterization of imexon-resistant RPMI8226/I myeloma cells. *Mol Cancer Ther* **1**, 185–195.

[17] Abramovitch R, Dafni H, Smouha E, Benjamin LE, and Neeman N (1999). In vivo prediction of vascular susceptibility to vascular endothelial growth factor withdrawal: magnetic resonance imaging of c6 rat glioma in nude mice. *Cancer Res* **59**, 5012–5016.

[18] Edrei Y, Gross E, Corchia N, Tsarfaty G, Galun E, Pappo O, and Abramovitch R (2011). Vascular profile characterization of liver tumors by magnetic resonance imaging using hemodynamic response imaging in mice. *Neoplasia* **13**, 244–253.

[19] Ogawa S, Lee TM, and Barrere B (1993). The sensitivity of magnetic resonance image signals of a rat brain to changes in the cerebral venous blood oxygenation. *Magn Reson Med* **29**, 205–210.

[20] Jagadish B, Guntle GP, Zhao D, Gokhale V, Ozumerzifon TJ, Ahad AM, Mash EA, and Raghunand N (2012). Redox-active magnetic resonance imaging contrast agents: studies with thiol-bearing 1,4,7,10-tetraazacyclododecane-1,4,7,10-tetracetic acid derivatives. *J Med Chem* **55**, 10378–10386.

[21] Raghunand N, Guntle GP, Gokhale V, Nichol G, Mash EA, and Jagadish B (2010). Design, synthesis, and evaluation of 1,4,7,10-tetraazacyclododecane-1,4,7-triacetic acid-derived, redox-sensitive contrast agents for magnetic resonance imaging. *J Med Chem* **53**, 6747–6757.

[22] Raghunand N, Jagadish B, Trouard TP, Galons JP, Gillies RJ, and Mash EA (2006). Redox-sensitive contrast agents for MRI based on reversible binding of thiols to serum albumin. *Magn Reson Med* **55**, 1272–1280.

[23] Menchise V, Digilio G, Gianolio E, Cittadino E, Catanzaro V, Carrera C, and Aime S (2011). In vivo labeling of B16 melanoma tumor xenograft with a thiol-reactive gadolinium based MRI contrast agent. *Mol Pharm* **8**, 1750–1756.

[24] Torres AG and Gait MJ (2012). Exploiting cell surface thiols to enhance cellular uptake. *Trends Biotechnol* **30**, 185–190.

[25] Robinson SP and Griffith JR (2004). Current issues in the utility of 19F nuclear magnetic resonance methodologies for the assessment of tumour hypoxia. *Philos Trans R Soc Lond B Biol Sci* **359**, 987–996.

[26] Pourpak A, Meyers RO, Samulitis BK, Chow HHS, Kepler CY, Raymond MA, Hersh E, and Dorr RT (2006). Preclinical antitumor activity, pharmacokinetics and pharmacodynamics of Imexon in mice. *Anti-Cancer Drugs* **17**, 1179–1184.

[27] Sengupta S, Chen H, Togawa T, DiBello PM, Majors AK, Budy B, Ketterer ME, and Jacobsen DW (2001). albumin thiolate anion is an intermediate in the formation of albumin-S–S-homocysteine. *J Biol Chem* **276**, 30111–30117.